Bulletin of the Disaster Prevention Research Institute Vol. 14, Part 2, February, 1965

76. Flow through Curved Open Channels

Part 1. On characteristics of upper layer in fully developed region

By Yoshio MURAMOTO

(Manuscript received October 2, 1964)

Abstract

This paper describes the hydraulic characteristics of the upper layer in a fully developed region of curved flow, as the first stage of the analytical approach to the general curved flow. On the basis of the fundamental equations of the upper layer unaffected by the wall shear, the effects of the secondary, radial flow on the main, tangential flow, and the variance of the hydraulic behaviors in curved flow with increase in centerline radius are discussed. Furthermore, the radial distribution of the tangential velocity and the surface profile derived from the present theory are examined in comparison with the experimental results in two kinds of test flumes with a single curved section of central angle 90° and 180°, respectively.

Resulting from the present study, it was confirmed that the existence of a fully developed region in the curved open channels is restricted to the latter portion of the curved section, and the experimental verification in this region supports present theory.

1. Introduction

It is generally considered that the curved reaches in rivers and canals are weak points of the structure which lead to undesirable situations, such as bank erosion, progression of meanders etc. Of no lesser importance is knowledge of the law of curved flows in the design of navigation and many other hydrotechnical structures.

For this reason, much effort has been devoted in the past to various laboratory studies and field investigations of the flow through curved channels. The remarkable phenomena in curved flows, as main subjects in previous studies, are as follows; (1) superelevation of the water surface, (2) behavior of secondary flows, (3) deviation of the high velocity filament to the outer bank, (4) development of separating regions, (5) local energy dissipation of curved flows.

All of these phenomena are essentially caused by the reciprocal action between a centripetal acceleration of fluid and frictional effects at the boundary. However, for lack of statistical fluid mechanics which describes the internal structure of non-homogeneous, or non-equilibrium flow field with mean hydraulic quantities, most previous studies stayed at the points of the qualitative explanation of the local phenomena in curved flows.

In the present study, as the first stage of the analytical approach to the general curved flow, the hydralic characteristics in the fully developed region of a circular curved reaches, which has a uniform equilibrium velocity distribution in the direction of the main flow, are considered. For this kind of curved flow, there are two useful approahes; the theory of laminar flow and

the theory of three-dimensional boundary layer.

The former approach is, as seen in previous studies[1),2),3),4)] on a curved pipe, only valid for the flow around gentle bends at a very small Reynolds number. Recently, a similar analytical method[5)] has been applied to obtain the secondary, transverse velocity profile of the turbulent flow in a curved open channel. However, even for gentle bends, it is impossible to determine the distribution of the main, longitudinal flow and the surface profile.

On the other hand, the latter approach is not restricted by the condition of the radius of bends and is applicable to turbulent flow, if we assume expressions for the velocity distribution and the shear stress in the bed. But, in previous studies[6),7),8),9)], the hydraulic behavior of the upper layer unaffected by the bed shear is not examined in detail, and the flow as a free vortex, or a forced vortex, was the main subject treated.

In this paper, the fundamental equations of the upper and lower layers are derived from the Navier-Stokes equation of motion and the approximate expression of continuity. As for the upper layer, the effects of the secondary flow on the main flow and the hydraulic characteristics of the variance of centerline radius are discussed. Further, on the basis of the experimental results in two kinds of test flumes with a single curved section, the existence of a fully developed region, the radial distribution of tangential velocity and the surface profile of the curved flow are verified.

2. Fundamental equations of curved flow

The equations of motion and continuity for a fully developed region of the curved flows are expressed by a system of cylindrical coordinates (θ, r, z) and corresponding components of velocity (u, v, w), as follows,

$$\begin{cases} v\dfrac{\partial u}{\partial r}+\dfrac{uv}{r}+w\dfrac{\partial u}{\partial z}=lg+\nu\left(\nabla^2 u-\dfrac{u}{r^2}\right), & (1)\\ v\dfrac{\partial v}{\partial r}-\dfrac{u^2}{r}+w\dfrac{\partial v}{\partial z}=mg-\dfrac{1}{\rho}\dfrac{\partial p}{\partial r}+\nu\left(\nabla^2 v-\dfrac{v}{r^2}\right), & (2)\\ 0=ng-\dfrac{1}{\rho}\dfrac{\partial p}{\partial z} & (3)\\ \dfrac{1}{r}\dfrac{\partial}{\partial r}(rv)+\dfrac{\partial w}{\partial z}=0. & (4) \end{cases}$$

l, m, n; directional cosine of gravitational acceleration for cylindrical coordinates, p: pressure with hydrostatic distribution along vertical axis z, ν; kinematic viscousity of fluid, and $\nabla^2=\dfrac{\partial^2}{\partial r^2}+\dfrac{1}{r}\dfrac{\partial}{\partial r}+\dfrac{\partial^2}{\partial z^2}$.

According to the boundary layer concept, the whole region of the flow is assumed to be divided into two layers; an upper layer which has a tangential velocity $U(r)$ and an outerward radial velocity $V(r)$, and a lower layer which is influenced by the frictional resistance of the channel bed and has a tangential velocity $u(r, z)$ and a radial velocity $v(r, z)$. At the boundary between the two layers, $z=\delta(r)$, three components of velocity are expressed by

$$u_\delta = U(r), \quad v_\delta = V(r) \qquad \text{and} \qquad w_\delta = -\frac{1}{r}\frac{\partial}{\partial r}\left(r\int_0^\delta v dz\right) + V\frac{\partial \delta}{\partial r}. \tag{5}$$

Considering these conditions, the momentum equations of two layers are obtained from Eqs. (1)～(4), for the upper layer

$$\begin{cases} \dfrac{1}{r^2}\dfrac{d}{dr}\{r^2 UV(h-\delta)\} + \dfrac{U}{r}\dfrac{d}{dr}\left(r\displaystyle\int_0^\delta v dz\right) \\ \qquad\qquad = (h-\delta)\left\{gl + \nu\left(\nabla_r^2 U - \dfrac{U}{r^2}\right)\right\}, \end{cases} \tag{6}$$

$$\begin{cases} \dfrac{1}{r}\dfrac{d}{dr}\{rV^2(h-\delta)\} - \dfrac{U^2}{r}(h-\delta) + \dfrac{V}{r}\dfrac{d}{dr}\left(r\displaystyle\int_0^\delta v dz\right) \\ \qquad\qquad = (h-\delta)\left\{gm + gn\dfrac{dh}{dr} + \nu\left(\nabla_r^2 V - \dfrac{V}{r^2}\right)\right\}, \end{cases} \tag{7}$$

and for the lower layer

$$\begin{cases} \dfrac{1}{r^2}\dfrac{d}{dr}\left(r^2\displaystyle\int_0^\delta uv dz\right) - \dfrac{U}{r}\dfrac{d}{dr}\left(r\displaystyle\int_0^\delta v dz\right) = gl\delta + \nu\displaystyle\int_0^\delta\left(\nabla^2 u - \dfrac{u}{r^2}\right)dz, \end{cases} \tag{8}$$

$$\begin{cases} \dfrac{1}{r}\dfrac{d}{dr}\left(r\displaystyle\int_0^\delta v^2 dz\right) - \dfrac{1}{r}\displaystyle\int_0^\delta u^2 dz - \dfrac{V}{r}\dfrac{d}{dr}\left(r\displaystyle\int_0^\delta v dz\right) \\ \qquad\qquad = g\delta\left(m + n\dfrac{dh}{dr}\right) + \nu\displaystyle\int_0^\delta\left(\nabla^2 v - \dfrac{v}{r^2}\right)dz, \end{cases} \tag{9}$$

in which h is the depth of flow and $\nabla_r^2 = d^2/dr^2 + d/rdr$. As seen from the left hand sides of Eqs. (6)～(9), the second term of Eq. (6) corresponds to the second term of Eq. (8) and the third term of Eq. (7) to the third term of Eq. (9), which indicates mutual interference of the momentum between the upper and the lower layer.

On the other hand, the expression of continuity in the whole region becomes from Eq. (4)

$$\frac{1}{r}\frac{d}{dr}\int_0^h rv dz = \frac{1}{r}\frac{d}{dr}r\left\{(h-\delta)V + \int_0^\delta v dz\right\} = 0, \tag{10}$$

and putting this relation into Eqs. (6) and (7), the equations of motion for the upper layer reduce to

$$\begin{cases} V\dfrac{dU}{dr} + \dfrac{UV}{r} = lg + \nu\left(\nabla_r^2 U - \dfrac{U}{r^2}\right), \end{cases} \tag{11}$$

$$\begin{cases} V\dfrac{dV}{dr} - \dfrac{U^2}{r} = mg + ng\dfrac{dh}{dr} + \nu\left(\nabla_r^2 V - \dfrac{V}{r^2}\right). \end{cases} \tag{12}$$

Consequently, according to the boundary layer theory, the fundamental equations of the curved flow are expressed by Eqs. (8)～(12). However, this system of differential equations cannot usually be solved, for the sake of the non-linear property of functions. Then, instead of Eq. (10) we introduce the assumption for the cotinuity between two layers,

$$\int_0^h v dz = 0, \tag{13}$$

and the equation of continuity for the upper layer,

$$\frac{1}{r}\frac{d}{dr}(rV)=0. \tag{14}$$

Eq. (13) is a sufficient condition of Eq. (10), and Eq. (14) is confirmed by the measurement of the radial velocity in the fully developed region of the curved flow.

3. Theoretical consideration of upper layer

3.1. Solutions of upper layer equations and effects of secondary flow.

In Eqs. (11) and (12), the viscous terms will be ignored except the region near the side walls and for the sake of simplicity, putting $l=i=$const. (=centerline slope of bed), $m=0$ and $n=-1$, the radial velocity, the tangential velocity and the depth of flow are obtained from Eqs. (11), (12) and (14), as follows,

$$V=C_1/r, \tag{15}$$

$$U=gir^2/3C_1+C_2/r, \tag{16}$$

$$h=gi^2r^4/36C_1^2-(C_1^2+C_2^2)/2gr^2+2iC_2r/3C_1+C_3, \tag{17}$$

in which C_1, C_2 and C_3 are integral constants. The superelevation of the water surface in the radial direction is given by

$$\Delta h=[h]_{r_1}^{r_2}=[gi^2r^4/36C_1^2-(C_1^2+C_2^2)/2gr^2+2iC_2r/3C_1]_{r_1}^{r_2}, \tag{18}$$

in which r_1 and r_2 refer to the inner and the outer radius of the curved section, respectively.

As deduced from Eqs. (15) and (16), the vorticity components (ξ, η, ζ), corresponding to the coordinates (θ, r, z) become

$$\xi=0,\quad \eta=0\quad\text{and}\quad \zeta=-\frac{1}{r}\frac{d}{dr}(Ur)=-\frac{gi}{V}=-\frac{gi}{C_1}r<0$$

which indicate a rotational flow with the vertical downward vorticity increased linearly to the radial direction.

The effects of the secondary flow on the main flow will be examined from a comparison between the present theory and the free-vortex theory. Against the velocity distribution of the free-vortex, the first term in Eq. (16), $gir^2/3C_1$ (>0) is added and expresses the effect to increase the tangential velocity to the outer bank. On the other hand, for the superelevation, the additional term in Eq. (18),

$$[gi^2r^4/36C_1^2-C_1^2/2gr^2+2giC_2r/3C_1]_{r_1}^{r_2}>0$$

shows the effect to increase superelevation by the secondary flow.

3.2. Relation between integral constants C_1 and C_2

In order to determine the characteristics of the curved flow from the results of the previous article, the integral constants C_1, C_2 and C_3 in Eqs. (15) ~(17) have to be evaluated by the boundary conditions of the side wall.

However, the behavior of the flow near the wall is so obscure that cannot be simplified to give the definite conditions of the velocity and the depth of flow.

Hence, to relate C_1 to C_2, we use the following assumption for the depth of flow, that is, "in one cross section of the curved flow, the mean depth ($\bar{h}$) coincides with the depth (h_c) at the centerline radius". According to the various experimental results, this assumption is valid for the flow through bend with any small radius, as long as a seperation zone is not present.

By the use of Eq. (17), putting $\bar{h}=h_c$, the following relation is obtained

$$\frac{1}{B}\int_{r_1}^{r_2}(n_1r^4-n_2/r^2+n_3r+C_3)\,dr=n_1r_c^4-n_2/r_c^2+n_3r_c+C_3,$$

in which B: the width of channel, r_c: the centerline radius, $n_1=gi^2/36C_1^2$, $n_2=(C_1^2+C_2^2)/2g$ and $n_3=2iC_2/3C_1$. After several calculations, the relation between C_1 and C_2 is expressed by

$$C_1^2(C_1^2+C_2^2)=-\frac{1}{9}g^2i^2B^6r_c'^2\left(r_c'^2+\frac{1}{40}\right)\left(r_c'^2-\frac{1}{4}\right), \tag{19}$$

where r_c' is a ratio of r_c/B ($>1/2$). Usually, C_1 is much less in magnitude than C_2 according to $V\ll U$ in the upper layer of the curved flow, so that by ignoring the term C_1^4 in Eq. (19), the approximate expression becomes

$$C_1C_2=\frac{1}{3}giB^3r_c'\sqrt{\left(r_c'^2+\frac{1}{40}\right)\left(r_c'^2-\frac{1}{4}\right)}. \tag{20}$$

Fig. 1 shows an example of the relation between C_1 and C_2 with parameter r_c' calculated from Eqs. (19) and (20) under conditions of $g=980$ cm/sec^2, $i=2\times10^{-3}$ and $B=25$ cm. Evidently, Eq. (20) may be applied instead of Eq. (19) for the region where C_2 is larger than C_1 in one order.

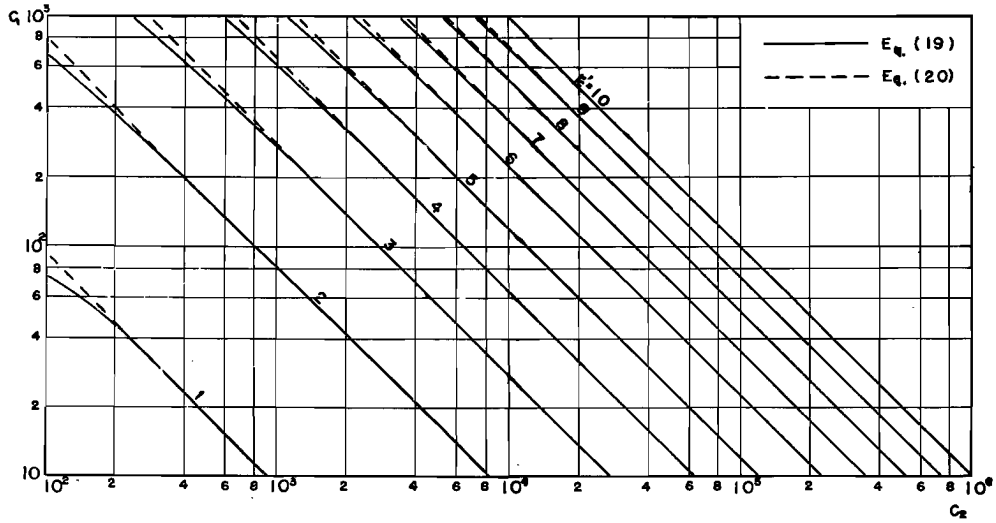

Fig. 1. An example of relation between C_1 and C_2 ($g=980$ cm/sec^2, $i=2\times10^{-3}$ and $B=25$ cm).

3.3. Tangential velocity and surface profile

General properties of tangential velocity and free surface profile with increase of the relative centerline radius r_c' are examined before the determination of the distribution of the tangential velocity and the surface profile.

By the use of Eqs. (16) and (20), the first derivative of the tangental velocity with respect to r is expressed by

$$\frac{dU}{dr}=\frac{2gi}{3C_1r^2}\left(r^3-\frac{3C_1C_2}{2gi}\right)=\frac{2gi}{3C_1r^2}\left\{r^3-\frac{1}{2}B^3r_c'\sqrt{\left(r_c'^2+\frac{1}{40}\right)\left(r_c'^2-\frac{1}{4}\right)}\right\}.$$

Accordingly, the condition $dU/dr\gtrless 0$ is dependent on

$$r'^3\gtrless\frac{1}{2}r_c'\sqrt{\left(r_c'^2+\frac{1}{40}\right)\left(r_c'^2-\frac{1}{4}\right)}, \tag{21}$$

where r' is a ratio of r/B and has the property $|r'-r_c'|\leqq 1/2$. An equality in Eq. (21) indicates the value of r' at the minimum value of U because of

$$\frac{d^2U}{dr^2}=\frac{2gi}{3C_1}+\frac{2C_2}{r^3}=\frac{2gi}{3C_1}\left\{1+\frac{1}{r'^3}r_c'\sqrt{\left(r_c'^2+\frac{1}{40}\right)\left(r_c'^2-\frac{1}{4}\right)}\right\}>0.$$

While, for the surface profile, derivating Eq. (16) twice with respect to r and eliminating C_2 on the basis of Eq. (19), the curvature of the free surface becomes

$$\frac{d^2h}{dr^2}=\frac{gi^2}{3C_1^2}\left\{r^2-\frac{9C_1^2(C_1^2+C_2^2)}{g^2i^2r^4}\right\}=\frac{gi^2}{3C_1^2r^4}\left\{r^6-B^6r_c'^2\left(r_c'^2+\frac{1}{40}\right)\left(r_c'^2-\frac{1}{4}\right)\right\},$$

and the condition $d^2h/dr^2\gtrless 0$ is given by

$$r'^3\gtrless r_c'\sqrt{\left(r_c'^2+\frac{1}{40}\right)\left(r_c'^2-\frac{1}{4}\right)}.$$

An equality in the above equation indicates the value of r' at the point of inflection of the surface profile.

Fig. 2 illustrates the characteristic diagram of the tangential velocity and the surface profile based on Eqs. (21) and (22). Region I and III have the properties of the flow similar to the forced vortex and the free vortex, respectively. Region II has a singular property combined both patterns.

(a) Tangential velocity : $U(r)$

As shown in Fig. 2, the distribution of the tangential velocity, with increase of the conterline radius, transfers from the region with $dU/dr\gtrless 0$ to the region

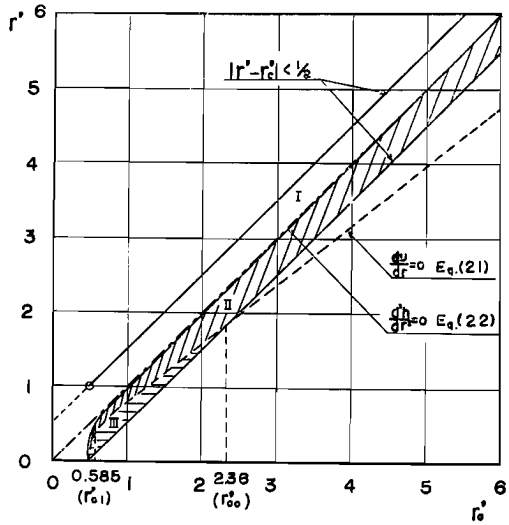

Fig. 2. Characteristic curves of $dU/dr=0$ [Eq. (21)] and $d^2h/dr^2=0$ [Eq. (22)] ($r_c'=r_c/B$, $r'=r/B$). Region I: $dU/dr>0$, $d^2h/dr^2>0$, Region II: $dU/dr>0$, $d^2h/dr^2<0$, Region III: $dU/dr<0$, $d^2h/dr^2<0$.

$dU/dr>0$. The latter region has been verified experimentally by many investigators and assumed as the flow with the velocity profile of the forced vortex, or proportional to r^n (n: positive constant value). On the other hand, the former region has not been detected by previous studies, but will be considered as the transitional region between the flows similar to the free vortex and the forced vortex. The value of r_c' at the boundary of two regions, r_{c0}', is calculated by Eq. (21) and the marginal condition of a channel $|r'-r_c'|=1/2$, as follows,

$$4(r_{c0}'-1/2)^6=r_{c0}'(r'^2_{c0}+1/40)(r'^2_{c0}-1/4),$$

and $r_{c0}'\fallingdotseq 2.36$.

Consequently, the maximum and the minimum values of U are determined separately for two regions, $0.5<r_c'\leqq 2.36$ and $2.36\leqq r_c'$.

(i) $0.5<r_c'\leqq 2.36$;

From Eqs. (16) and (21), the minimum value of U becomes

$$U_{min}=\frac{giB^2}{3C_1}\left\{r_0'^2+r'_c\sqrt{\left(r_c'^2+\frac{1}{40}\right)\left(r_c'^2-\frac{1}{4}\right)}\right\}, \tag{23}$$

in which $r_0'=\sqrt[6]{r_c'^2(r_c'^2+1/40)(r_c'-1/4)/4}$.

The maximum value of U exists at the inner or the outer bank, and the value of r_c' at the condition $U_1=U_2$, where subscriptions 1 and 2 refer to the inner and the outer bank, r_{c1}', is obtained from

$$U_2-U_1=\frac{C_2}{12(r_{c1}'^2-1/4)B}\left\{8\frac{r_{c1}'-1/4}{\sqrt{(r_{c1}'^2+1/40)(r_{c1}'^2-1/4)}}-4\right\}=0,$$

and $r_{c1}'\fallingdotseq 0.585$. Hence, the maximum value of U becomes for $0.5<r_c'\leqq 0.585$,

$$U_{max}=U_1=\frac{giB^2}{3C_1}\left\{\frac{(r_c'-1/2)^3+r_c'\sqrt{(r_c'^2+1/40)(r_c'^2-1/4)}}{r_c'-1/2}\right\}, \tag{24}$$

and for $0.585\leqq r_c'\leqq 2.36$,

$$U_{max}=U_2=\frac{giB^2}{3C_1}\left\{\frac{(r_c'+1/2)^3+r_c'\sqrt{(r_c'^2+1/40)(r_c'^2-1/4)}}{r_c'+1/2}\right\}. \tag{25}$$

(ii) $2.36\leqq r_c'$;

In this region, evidently the maximum and the minimum values of U are given by Eqs. (24) and (25), respectively. However, at the large value of r_c', Eq. (20) is developed in series,

$$C_1C_2=\frac{gir_c^3}{3}\left\{1-\frac{9}{80r_c'^2}-\frac{1}{640r_c'^4}-O\left(\frac{1}{r_c'^6}\right)\right\},$$

and the following approximation may be adopted

for $2\leqq r_c'<5$, $$C_1C_2\fallingdotseq\frac{gir_c^3}{3}\left(1-\frac{9}{80r_c'^2}\right) \tag{20}'$$

and for $r_c'\geqq 5$, $$C_1C_2\fallingdotseq gir_c^3/3. \tag{20}''$$

Under considerations of the approximation in Eqs. (24) and (25), the maximum and the minimum values of U become

for $2 \leqq r_c' < 5$, $$U_{min} = U_1 \fallingdotseq \frac{giB^2}{3C_1}\left\{\left(r_c' - \frac{1}{2}\right)^2 + \frac{r_c'(r_c'^2 - 9/80)}{r_c' - 1/12}\right\}, \tag{26}$$

$$U_{max} = U_2 \fallingdotseq \frac{giB^2}{3C_1}\left\{\left(r_c' + \frac{1}{2}\right)^2 + \frac{r_c'(r_c'^2 - 9/80)}{r_c' + 1/12}\right\}, \tag{27}$$

and for $r_c' \geqq 5$. $$U_{min} = U_1 \fallingdotseq \frac{giB^2}{3C_1}\left\{\left(r_c' - \frac{1}{2}\right)^2 + \frac{r_c'^3}{r_c' - 1/12}\right\}, \tag{26}'$$

$$U_{max} = U_2 \fallingdotseq \frac{giB^2}{3C_1}\left\{\left(r_c' + \frac{1}{2}\right)^2 + \frac{r_c'^3}{r_c' + 1/12}\right\}, \tag{27}'$$

Now, from Eqs. (16) and (21), a non-dimensional expression of U is given by

$$\frac{U}{U_c} = \frac{r'^3 + r_c'\sqrt{(r_c'^2 + 1/40)(r_c'^2 - 1/4)}}{r_c'^3 + r_c'\sqrt{(r_c'^2 + 1/40)(r_c'^2 - 1/4)}} \cdot \frac{r_c'}{r'}, \tag{28}$$

where U_c is the velocity at the centerline radius. For the large value of r_c', using Eqs. (20)′ and (20), Eq. (28) becomes

for $2 \leqq r_c' < 5$, $$\frac{U}{U_c} \fallingdotseq \frac{r'^3 + r_c'(r_c'^2 - 9/80)}{(2r_c' - 9/80)r'}, \tag{28}'$$

and for $r_c' \geqq 5$, $$\frac{U}{U_c} \fallingdotseq \frac{1}{2}\left(\frac{r'^2}{r_c'^2} + \frac{r_c'}{r'}\right). \tag{28}''$$

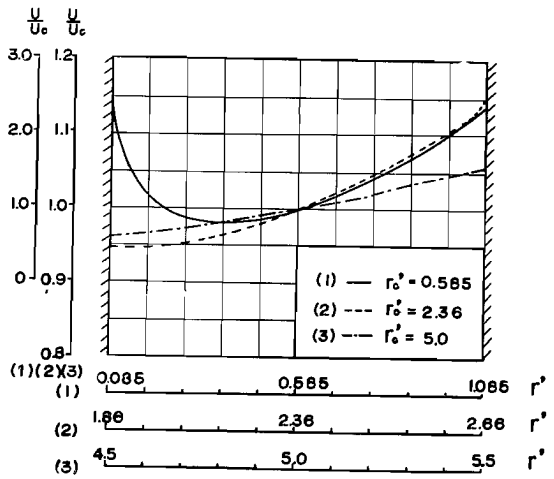

Fig. 3. Typical examples of tangential velocity profiles [Eq. (28)].

Fig. 3 indicates typical examples of the velocity profiles for $r_c' = r_{c1}' = 0.585$, $r_c' = r_{c0}' = 2.36$ and $r_c' = 5$ calculated from Eqs. (28)～(28)″.

(b) Surface profile : $h(r)$

As shown in Fig. 2, for all r_c' larger than 0.5, the value of (d^2h/dr^2) varies from the negative to the positive sign approximately at the point of the centerline, so that the surface profile varies from a convex shape to a concave shape. And, the point of inflection is almost consistent with the centerline radius for $r_c' \geqq 5$.

By the use of Eqs. (17) and (20), a non-dimensional expression of the surface profile is given by

$$\frac{h - h_c}{B} = \frac{gi^2B^3}{36C_1^2}\left\{r'^4 - 2r_c'^2\left(r_c'^2 + \frac{1}{40}\right)\left(r_c'^2 - \frac{1}{4}\right)\frac{1}{r'^2} + 8r_c'\sqrt{\left(r_c'^2 + \frac{1}{40}\right)\left(r_c'^2 - \frac{1}{4}\right)}r'\right.$$
$$\left. - r_c'^4 + 2\left(r_c'^2 + \frac{1}{40}\right)\left(r_c'^2 - \frac{1}{4}\right) - 8r_c'^2\sqrt{\left(r_c'^2 + \frac{1}{40}\right)\left(r_c'^2 - \frac{1}{4}\right)}\right\}, \tag{29}$$

and the approximate expressions become

$$\text{for } 2\leqq r_c'<5, \quad \frac{h-h_c}{B}\fallingdotseq\frac{gi^2B^3}{36C_1^2}\left\{r'^4-\left(2r_c'^6-\frac{9}{20}r_c'^4\right)\frac{1}{r'^2}+8\left(r_c'^3-\frac{9}{80}r_c'\right)r'-7r_c'^4+\frac{9}{10}r_c'^2\right\}, \tag{29}'$$

$$\text{and for } r_c'\geqq 5, \quad \frac{h-h_c}{B}\fallingdotseq\frac{gi^2B^3}{36C_1^2}\left(r'^4-2r_c'^6\frac{1}{r'^2}+8r_c'^3r'-7r_c'^4\right) \tag{29}''$$

Some examples of surface profiles obtained from Eqs. (29)～(29)'' are shown in Fig. 4 under conditions of $g=980$ cm/sec², $i=2\times10^{-3}$, $B=25$ cm and $C_1=10$, 10^2, $10^{5/2}$ for $r_c'=0.585$, 2.36, 5.0, respectively. The variance in the curvature of the surface profile is remarkable for the small value of r_c', but, for the large r_c', it will be difficult to detect the point of inflection by the usual experimental methods.

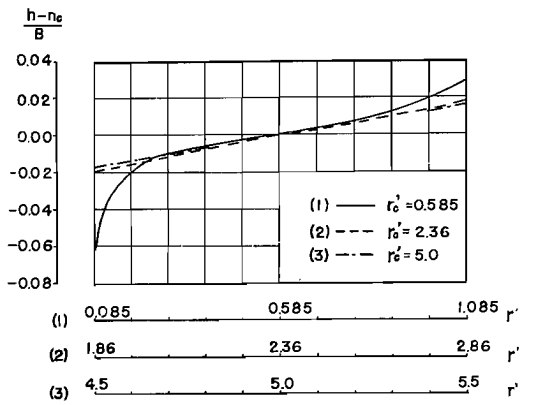

Fig. 4. Typical examples of water surface profiles [Eq. (29)].

On the other hand, the superelevation of water surface is obtained from Eqs. (18) (20), as follows,

$$\Delta h=\frac{gi^2B^4}{9C_1^2}r_c'\left\{2r_c'^2+r_c'\sqrt{\left(r_c'^2+\frac{1}{40}\right)\left(r_c'^2-\frac{1}{4}\right)}+\frac{11r_c'^2}{40(r_c'^2-1/4)}+\frac{1}{4}\right\}, \tag{30}$$

and the approximate expressions become

$$\text{for } 2\leqq r_c'<5, \quad \Delta h=\frac{gi^2B^4}{9C_1^2}r_c'\left(3r_c'^2+\frac{11}{20}\right), \tag{30}'$$

$$\text{and for } r_c'\geqq 5, \quad \Delta h=\frac{gi^2B^4}{3C_1^2}r_c'^3. \tag{30}''$$

4. Experimental Verification

4.1. Experimental equipment

The experiments were conducted in two kinds of flumes; a curved flume with lucite walls at the Hydraulic Laboratory in Engineering Research Institute, and a curved concrete flume at Ujigawa Hydraulic Laboratory in the Disaster Prevention Research Institute.

The former flume has a uniform rectangular cross section 25 cm in width and 37 cm in height. It consists of four straight sections, and eight curved sections with 90° and 180° central angle and, each other, four kinds of centerline radius that can be composed to give any desired alinement. The alinements adopted in this study consist of a straight approach section 10.25 m in length, one of the four curved sections with $\theta=90°$, in central angle,

and a straight 4.25 m exit section. Four kinds of the centerline radii in the curved section are $r_c=25$ cm, 50 cm, 75 cm and 100 cm, namely, the relative radii $r_c'=1$, 2, 3 and 4, respectively. And, the centerline slope was set at 0.002 during this experimental program.

The latter flume is constructed of a uniform rectangular cross section 50 cm in width and 30 cm in height. It consists of a straight 9 m approach section, a single curve of central angle $\Theta=180°$ and 150 cm in centerline radius, namely, $r_c'=3$, and a stright 10 m exit section. The centerline slope was also set at 0.002.

For the expriments in both flumes, flow depths were measured with point gauges to an accuracy of 1/10 mm and velocities of the main flow with round-nosed Prandtl tubes with 3 mm in diameter. Further, in order to indirectly determine the radial and the vertical velocities, three-dimensional flow directions were measured by the use of a cylindrical pitot tube with two holes in a horizontal plane and a pitot sphere with five holes.

In the next two articles, on the basis of the experimental results in two curved flumes, assumptions and the theoretical considerations for the flow in the upper layer will be discussed.

4.2. Experimental verification of 90° bend

Fig. 5 presents the experimental verification of the assumption, $\bar{h}=h_c$, for the flow depth in the previous section [3.2]. If the water surface in the curved section has a profile as a free vortex, the relation between $\bar{h}$ and h_c will always be $\bar{h}<h_c$ because of $d^2h/dr^2<0$. And, if it has a profile of a forced vortex, the inequality will be $\bar{h}>h_c$ because of $d^2h/dr^2>0$. The experimental values are in accordance with the straight line of $\bar{h}=h_c$ for any case of r_c', and indicate justification for the assumption. Other than at the station $\theta=90°$, it is proved by further experimental results that this assumption will be able to used even for the undeveloped region without a separation zone.

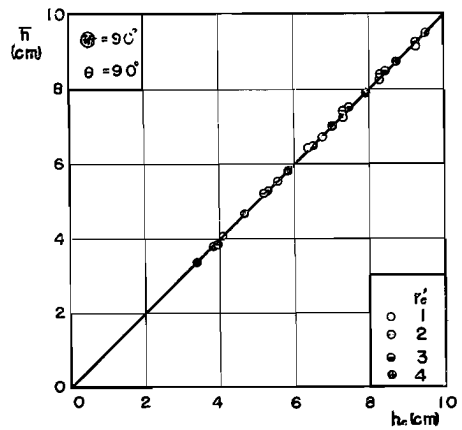

Fig. 5. Experimental verification of assumption, $\bar{h}=h_c$.

In Fig. 6, the theoretical curves related C_1 to C_2 [Eq. (19)] are compared with the experimental values, that are calculated from Eqs. (15) and (16) by the use of the observed values of the tangential velocities and the flow directions in a horizontal plane. Any decrease of r_c', that is, increase of the curvature of the curved section, is seen as a larger deviation from theoretical curves. Probably, it is considered that in the small value of r_c', the development of the secondary flow is not enough to establish the equilibrium region of the curved flow within 90° bend. This property for the development of the curved flow is also illustrated from the variation of the tangential velocity profile within the bend.

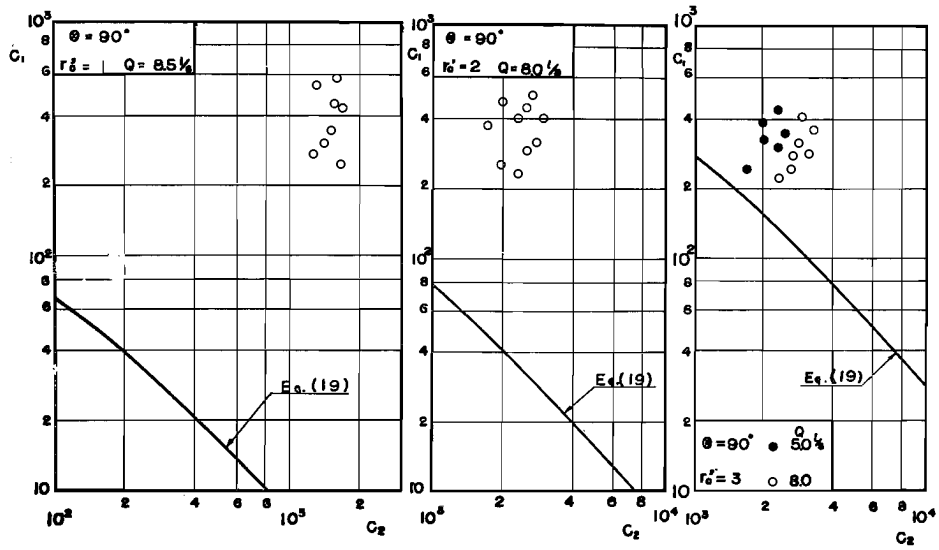

Fig. 6. Comparison between theoretical curves [Eq. (19)] and observed values for relationship C_1 to C_2.

For the different values of $r_c'=1\sim4$, the observed radial distributions of the tangential velocity at three stations, $\theta=30°$, 60° and 90°, from beginning of bend, are shown in Figs. 7-1~7-4. Three curves in these figures indicate non-dimensional expressions of the velocity profiles as a free vortex $U/U_c=r_c'/r'$, as a forced vortex $U/U_c=r'/r_c'$, and Eq. (28) derived in the previous section.

In the cases of $r_c'=1\sim3$, the observed distributions at $\theta=30°$ and 60° illustrate the deviation of the higher velocity filament to the inner bank similar

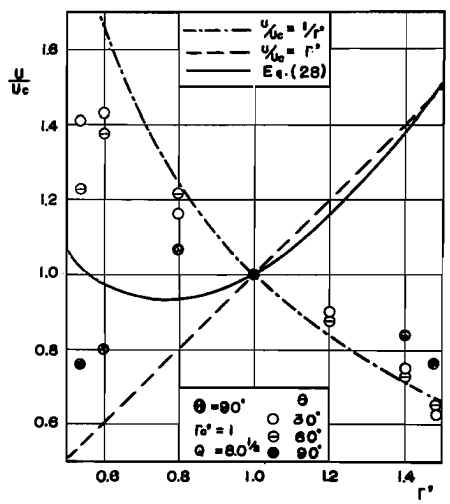

Fig. 7-1.

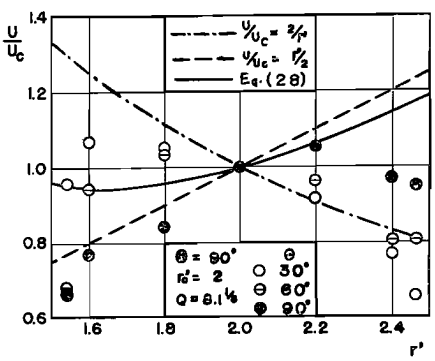

Fig. 7-2.

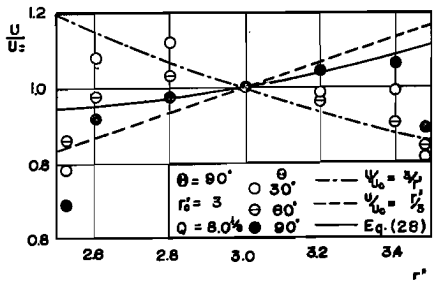

Fig. 7-3.

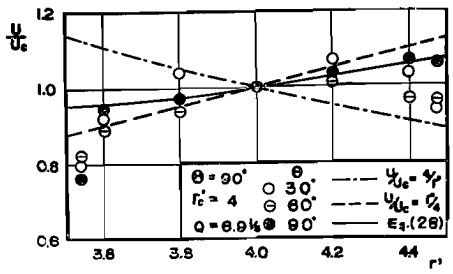

Fig. 7-4.

Figs. 7-1~7-4. Comparison between theoretical velocity profiles and experimental data at $\theta=30°\sim90°$.

to the free-vortex pattern, but its formula is only valid in the case $r_c'=1$. And, the forced vortex formula is not valid in any case. The validity of the theoretical curves based on Eq. (28), however, is only recognized at $\theta=90°$ in the cases $r_c'=3$ and 4. Accordingly, as in the argument in Fig. 6, the equilibrium region with fully developed secondary flow will be restricted near the exit section of bend with the value of r_c' larger than 3.

Figs. 8-1~8-4 show the comparisons between the observed surface profiles at $\theta=90°$ and the theoretical profiles based on Eq. (29), in which C_1 is cal-

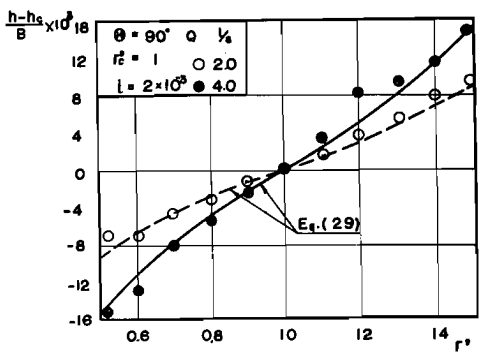

Fig. 8-1.

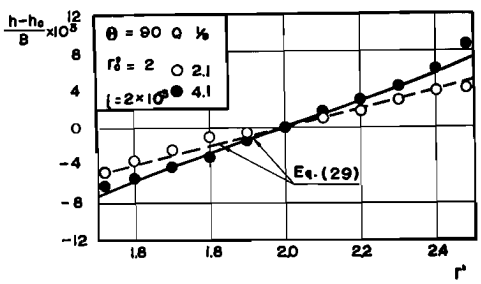

Fig. 8-2.

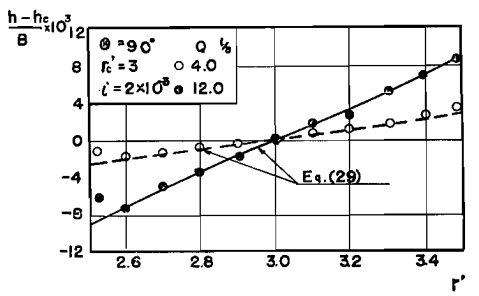

Fig. 8-3.

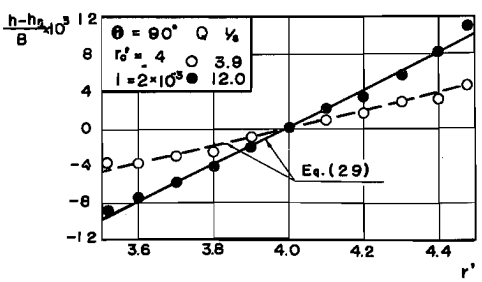

Fig. 8-4.

Figs. 8-1.~8-4. Comparison between theoretical surface profile and experimental data.

culated from Eqs. (16) and (20) by the use of the experimental values of the tangential velocity. In all cases of $r_c'=1\sim4$, agreement between them is fairly good except near the side walls.

4.3. Experimental verification of 180° band

In Fig. 9, the assumption $\bar{h}=h_c$ is examined by the experimental values of flow depth at $\theta=90°\sim180°$ with the range of discharge, $Q=5\sim30$ l/sec. Accordance between them is fairly good within the accuracy of our measuring apparatus.

Figs. 10 and 11 give the observed radial distribution of the tangential velocity at different stations and with different discharges, in comparison with

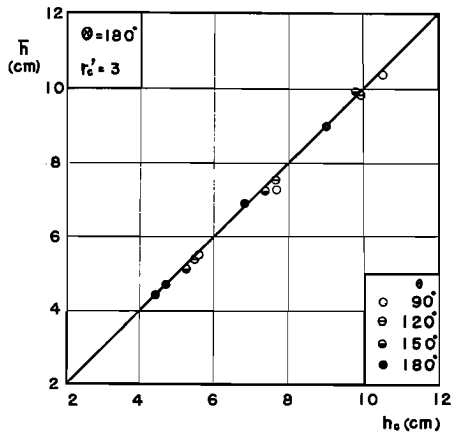

Fig. 9. Experimental verification of assumption, $\bar{h}=h_c$.

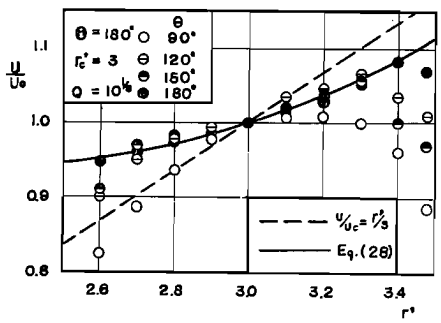

Fig. 10. Comparison between theoretical velocity profile and experimental data with constant discharge at different stations.

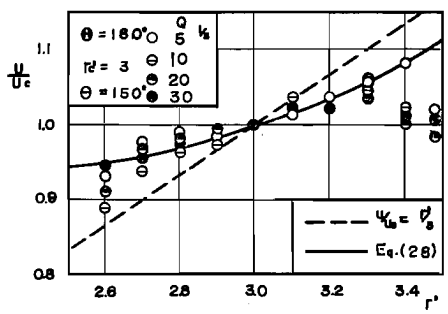

Fig. 11. Comparison between theoretical velocity profile and experimental data for different discharges, at $\theta=150$.

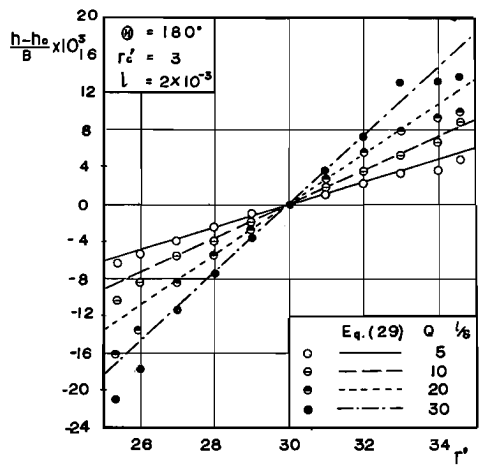

Fig. 12. Comparisons between theoretical surface profile and experimental data with different discharges.

the forced vortex formula and Eq. (28). As shown in Fig. 10, except near the side walls, the experimental values at $\theta=120°\sim180°$ coincide with the curve of Eq. (28) rather than that of forced vortex formula. While, Fig. 11 illustrates that the velocity profile given by the non-dimensional expression, U/U_c, will be independent of the rate of discharge in accordance with the form of Eq. (28). Accordingly, the fully developed region is considered to exist in the reach $\theta\fallingdotseq120°\sim180°$ for this bend.

Lastly, in Fig. 12, the theoretical surface profiles are compared with the experimental values at $\theta=150°$ for the different discharges, $Q=5\sim30$ l/sec. Although, for the case of the larger discharge, the slight deviation from the predicted curve is seen to be due to the higher disturbance of surface, both theoretical and experimental results are to be in good agreement except for those near the wall.

5. Conclusion

The hydraulic characteristics of the upper layer in the fully developed region are discussed in detail, as the first report of the research program on the internal structure of the flow through curved open channels.

In consequence of the present study, an illustration was given of the theory that the secondary flow has influence upon the main flow in shifting the higher velocity filament to the outer bank and in increasing the superelevation of the water surface. Further, the existences of the fully developed region, the theoretical distribution of the tangential velocity and the surface profile were confirmed by experimental results in two kinds of curved flumes.

Hereafter, on the basis of the present study, the hydraulic behaviors of the flow near the wall affected by the shear force will be examined.

Acknowledgment

The author would like to express his sincere appreciation to Professor Tojiro Ishihara for his approval in the preparation of this paper. Thanks are also expressed to Mr. S. Ishida, Mr. T. Inoue and Mr. K. Mashima for their helpful assistance in experiments and calculations.

References

1) Boussinesq, J. : Jour. Math. Appliq., Sér. 12, Tome XIII, 1868.
2) Dean, W. R. : Phil. Mag., S. 7, Vol. 4, 208, 1927.
3) Dean, W. R. : Phil. Mag., S. 7, Vol. 5, 673, 1928.
4) Ito, H. : Rep. Inst. High Sp. Mech., Tōhoku Univ., 1, 1951.
5) Rozovskii, I. L. : "Flow of Water in Bends of Open Channels", Acade. Sci. Ukrainian, SSR, 1957.
6) Ito, H. : Trans. ASME, Ser. D, 81-2, 123, 1959.
7) Einstein, H. A. and Harder, I. A. : Trans. AGU, Vol. 35, No. 1, 114, 1954.
8) Iwagaki, Y. : "Applied Hydraulics" 2nd Vol., Part II, 78-80, Maruzen, 1958.
9) Kishi, T. and Ogawa, Y. : Proc. 7th Hydraulic Symposium, JSCE, 71, 1962.
10) Muramoto, Y. and Ishida, S. : Disaster Prevention Research Institute Annuals, No. 7, 315-328, 1964.